SCIENCE CHINA
Technological Sciences

•Article•

October 2022 Vol.65 No.10: 2503–2519
https://doi.org/10.1007/s11431-022-2158-9

Analytical solutions for deep tunnels in strain-softening rocks modeled by different elastic strain definitions with the unified strength theory

SUN ZhenYu[1], ZHANG DingLi[1*], FANG Qian[1], DUI GuanSuo[1] & CHU ZhaoFei[2]

[1] *Key Laboratory for Urban Underground Engineering of Ministry of Education, Beijing Jiaotong University, Beijing 100044, China;*
[2] *School of Civil Engineering, Wuhan University, Wuhan 430072, China*

Received June 6, 2022; accepted July 22, 2022; published online July 30, 2022

This paper presents the analytical solutions for the responses of tunnels excavated in rock masses exhibiting strain-softening behavior. Since previous analyses give little consideration to the effect of the intermediate principal stress on the strain-softening rock behavior, the unified strength theory was introduced to analyze the tunnel response. Four cases of different definitions of the elastic strain in the softening and residual regions, used in the existing solutions, were considered. The tunnel displacements, stresses, radii of the softening and residual zones and critical stresses were deduced. The proposed solutions were verified by comparing with numerical simulations, model tests and existing solutions. Furthermore, the solutions of the four cases were compared with each other to investigate the influence of the elastic strain expressions on the tunnel responses. The results showed that the intermediate principal stress coefficient b has a significant effect on the tunnel displacements, stress fields, and plastic radii. Parametric studies were performed to analyze the influences of the softening and residual dilatancy coefficients, softening modulus and residual strength on the tunnel responses. The parametric analysis indicated that the existing models should be carefully evaluated in the analysis of tunnels constructed through average-quality rocks; the proposed solutions outperformed the existing models in solving the mentioned problem.

analytical solution, elastic strain definition, unified strength theory, strain-softening, intermediate principal stress, model test

Citation: Sun Z Y, Zhang D L, Fang Q, et al. Analytical solutions for deep tunnels in strain-softening rocks modeled by different elastic strain definitions with the unified strength theory. Sci China Tech Sci, 2022, 65: 2503–2519, https://doi.org/10.1007/s11431-022-2158-9

1 Introduction

Tunnel responses such as displacements, stresses and plastic radii are crucial factors in the analysis of surrounding rock stability and quantitative support design. Three different types of approaches are being currently used to predict tunnel responses: theoretical analysis, numerical simulation and model testing. These three approaches are considered complementary to each other in tunnel design, while theoretical analysis provides research benchmarks for numerical simulation and model test methods, which plays an irreplaceable role in grasping the essence of the problems and has been widely used in the preliminary design [1–4].

Over the past few decades, the theoretical analyses of tunnels have been mainly based on Mohr-Coulomb (M-C) and Hoek-Brown (H-B) criteria. The different behaviors of rock masses, such as the elastic perfect plastic [5–7], strain softening [8–11], hardening [12–14], elastic-brittle plastic [15–17] and elastic-plastic-viscous [18–20] have been modeled and solved. However, neither the M-C criterion nor the H-B criterion considers the effect of the intermediate principal stress. In fact, the rock mass strength is often ob-

*Corresponding author (email: dlzhang@bjtu.edu.cn)

served to be dependent on the intermediate principal stress, and this effect is associated with the rock mass properties and stress states [21–27]. The unified strength theory (UST), which considers all the stress components and their effects on the material yield and failure, can quantify the effect of the intermediate principal stress of various materials with different stress states and take full advantage of the material strength [28–32]. In the past twenty years, the UST has attracted extensive attention and has been used in several fields such as tunnel engineering, geotechnical engineering, and geological engineering [33–41].

In the elastoplastic analysis of tunnel responses, it is necessary to assume the expression of the elastic strain in the plastic zone. There are generally four definitions of the elastic strain in the plastic zone in existing analyses: ignoring the elastic strain [42–44], treating it as a constant [45,46], considering the plastic zone as a thick-walled cylinder [47,48] and obtaining it using the Hooke's law [49,50]. Different elastic strain assumptions cause significant differences in the calculation results of surrounding rock deformation, which will affect the support design. In fact, there is no consensus on which definition should be adopted for rock masses with different qualities. However, all existing research used one or some of the above-mentioned expressions of the elastic strain in the plastic zone, which is not comprehensive and not conducive to tunnel design.

In addition, the post failure behavior of the rock mass has significant effect on the tunnel responses. Many researchers have developed a variety of methods for the plastic problems of tunnelling, but mainly for elastic-perfectly-plastic or elastic-brittle rock masses. In some cases, however, the elastic-perfectly-plastic or elastic-brittle model were inappropriate to describe the post-failure behavior of a material, particularly in the case of average-quality rock masses [51,52]; the average-quality rock masses, with a geological strength index (GSI) of $40 < \mathrm{GSI} < 60$, would behave in a strain-softening instead. Indeed, both elastic-perfectly-plastic and elastic-brittle models are special cases of the strain-softening model and thus, it is important to investigate the tunnel responses in strain-softening rock masses. In this regard, there has been no research considering the effect of the intermediate principal stress in the strain-softening rock mass under different definitions of the elastic strain. The effects of the residual dilatancy, cohesion and friction angle on the tunnel responses remain unclear.

In this study, the UST is introduced in the derivation of the tunnel responses accounting for the effect of the intermediate principal stress. Based on four definitions of the elastic strain, analytical solutions are presented for the displacements, stress fields, plastic radii and critical stresses of deep tunnels excavated in strain-softening rock masses. To investigate the effects of the intermediate principal stress and different definitions of the elastic strains on the tunnel responses, the derived solutions are compared with the solutions proposed by Yao et al. [53] based on the M-C criterion and by Zhang et al. [54] who used the UST elastic-brittle-plastic model. In addition, parametric analysis of the proposed solutions, such as the influence of the dilatancy, softening modulus, residual cohesion and friction angle on the tunnel displacements, stress fields and plastic radii, was performed.

2 Problem definition and basic assumptions

2.1 Strain-softening model

Figure 1 shows a deep circular tunnel excavated in a homogeneous and isotropic rock mass with the radius r_0 in the plane strain state. The tunnel is subjected to a hydrostatic stress p_0 at infinity and a uniformly distributed pressure p_i at the internal surface. With the decrease in p_i, the softening zone appears when p_i is less than the initial yielding stress p_s. After yielding, the rock strength gradually decreases from the peak value σ_q and follows the post-peak softening behavior. When p_i decreases to the critical stress p_r, the residual zone appears with the residual strength being σ_{qr}.

Figure 2 shows the trilinear constitutive relationship of a strain-softening material used in this study [55–57]. The compressive stress components and the inward tunnel displacement are counted positive. The elastic behavior is governed by Hooke's law, whereas the plastic behavior is assumed to obey the UST with unassociated flow rules. To solve the proposed problem, four different cases of the definition of the elastic strain in the plastic zones (both the softening and residual zones) are distinguished as follows:

Case a: Elastic strains are ignored in the plastic zones;

Case b: Elastic strains are constant in the plastic zones;

Case c: Elastic strains are obtained by considering the plastic zones as the thick-walled cylinder;

Case d: Elastic strains are obtained using the Hooke's law.

Among all the cases, Cases a, b and c are approximations, while Case d is an exact solution to the radial displacement [15,49].

2.2 Unified strength theory

The UST proposed by Yu [58] assumes that a material begins to yield when the sum of the two greater principal shear stresses and the corresponding normal stress functions reach certain values. Since it considers all the stress components and their effects on the yield and failure of materials, the theory is suitable for geomaterials with different tensile and compressive strengths, which can appropriately reflect the effect of the intermediate principal stress. The UST refers to a series of constitutive models related to the value of the intermediate principal stress coefficient b, as shown in

Figure 3.

As two special cases, the M-C criterion and the twin-shear criterion can be obtained when $b = 0$ and $b = 1$, respectively.

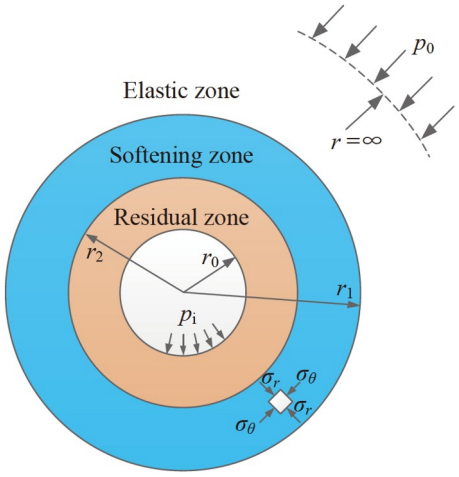

Figure 1 (Color online) Sketch of the tunnel surrounding rock exhibiting strain-softening behavior.

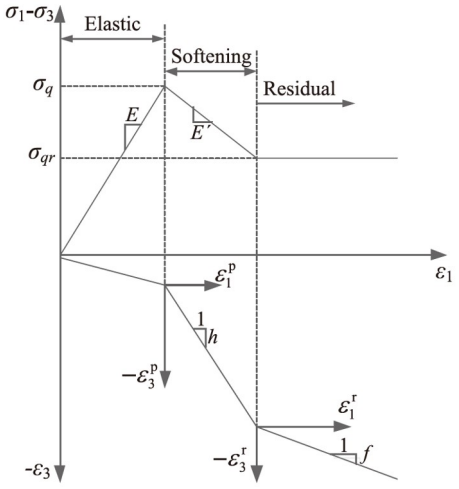

Figure 2 Constitutive relationship of a strain-softening material.

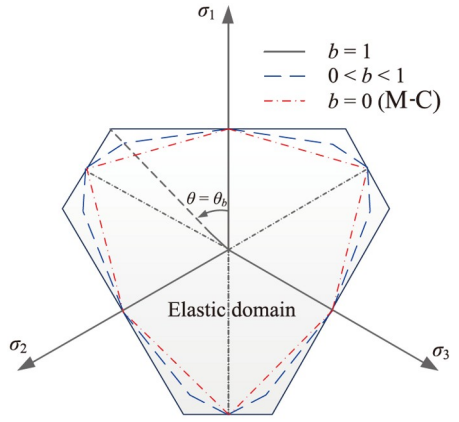

Figure 3 (Color online) Unified strength theory in the deviatoric plane.

The UST can be expressed in terms of the three principal stresses as follows [58]:

$$\begin{cases} F' = a\sigma_1 - \dfrac{1}{1+b}(b\sigma_2+\sigma_3) - \sigma_t, & \sigma_2 \le d, \\ F = \dfrac{a}{1+b}(\sigma_1 + b\sigma_2) - \sigma_3 - \sigma_t, & \sigma_2 \ge d, \end{cases} \tag{1}$$

where σ_1, σ_2 and σ_3 are the maximum, intermediate and minimum principal stresses, respectively; a is the ratio of tensile strength σ_t to the compressive strength σ_c. $\sigma_t = \dfrac{2c\cos\varphi}{1+\sin\varphi}$ and $\sigma_c = \dfrac{2c\cos\varphi}{1-\sin\varphi}$. c and φ are the cohesion and friction angle, respectively. d is the demarcation point of the domain and $d = \dfrac{a\sigma_1+\sigma_3}{1+a}$.

For the plane strain problem, the intermediate principal stress σ_2 can be expressed by σ_1 and σ_3 as [58]

$$\sigma_2 = \frac{m}{2}(\sigma_1+\sigma_3), \tag{2}$$

where m is an empirical constant, the magnitude of which is equal to 2μ in the elastic state and quite close to 1 in the plastic state. μ is the Poisson's ratio.

Accordingly, we have

$$\sigma_2 = \frac{m}{2}(\sigma_1+\sigma_3) \approx \frac{1}{2}(\sigma_1+\sigma_3). \tag{3}$$

Substituting $a = \dfrac{\sigma_t}{\sigma_c}$ into the demarcation point of the domain, d can be reformulated as

$$d = \frac{1}{2}(\sigma_1+\sigma_3) - \frac{\sin\varphi}{2}(\sigma_1-\sigma_3). \tag{4}$$

Since $\sin\varphi > 0$ and $\sigma_1 \ge \sigma_3$, d is always lower that the rightmost-hand side of eq. (3). Combining eqs. (3) and (4) results in $\sigma_2 \ge d$. Under the assumptions made in this study, the principal stress σ_θ, the radial stress σ_r and axial stress σ_z are the major, minor and intermediate stresses, respectively. Based on the mechanical model used here, the UST can be written as

$$\begin{cases} F = \sigma_\theta - \xi_0\sigma_r - \sigma_{cq} = 0, \\ \sigma_{cq} = \sigma_q - E'\varepsilon_\theta^p, \end{cases} \text{ for the softening zone,} \tag{5}$$

$$F = \sigma_\theta - \xi_r\sigma_r - \sigma_{qr} = 0, \text{ for the residual zone,} \tag{6}$$

where E' is the unified softening modulus. σ_q, σ_{cq} and σ_{qr} are the unified peak strength, rock strength in the softening zone and residual strength, respectively. ξ_0 and ξ_r are constants which can be expressed as

$$\begin{cases} \xi_0 = \dfrac{2(1+b)(1+\sin\varphi_0) - bm(1-\sin\varphi_0)}{(2+bm)(1-\sin\varphi_0)}, \\ \sigma_q = \dfrac{4(1+b)c_0\cos\varphi_0}{(2+bm)(1-\sin\varphi_0)}, \\ \xi_r = \dfrac{2(1+b)(1+\sin\varphi_r) - bm(1-\sin\varphi_r)}{(2+bm)(1-\sin\varphi_r)}, \\ \sigma_{qr} = \dfrac{4(1+b)c_r\cos\varphi_r}{(2+bm)(1-\sin\varphi_r)}, \end{cases} \tag{7}$$

where c_0 and φ_0 are the unified cohesion and friction angle in the softening zone, respectively. c_r and φ_r are the unified residual values of the cohesion and friction angle of the rock, respectively.

3 Derivation of the stress and displacement of deep circular tunnels

3.1 Analytical solution for the elastic zone

For the axial symmetry of the problem, the differential equilibrium equation can be expressed as

$$\frac{\mathrm{d}\sigma_r}{\mathrm{d}r}+\frac{\sigma_r-\sigma_\theta}{r}=0. \tag{8}$$

The displacement in the elastic zone of surrounding rock can be expressed as [5]

$$u_r=\frac{A}{Er}(1+\mu), \tag{9}$$

where E is the elasticity modulus of the surrounding rock. A is a coefficient to be determined and $A=(p_0-p_i)r_0$ when there is no softening zone.

Substituting $r=r_1$, $u_r=u_{r_1}$ into eq. (9) yields

$$u_{r_1}=\frac{A}{Er_1}(1+\mu), \tag{10}$$

where r_1 is the radius of the softening zone.

Substituting eq. (10) into eq. (9) yields

$$u_r=u_{r_1}\frac{r_1}{r}. \tag{11}$$

The stresses in the elastic zone can be expressed as [59]

$$\begin{cases}\sigma_r^e=-\dfrac{u_{r_1}Er_1}{(1+\mu)r^2}+p_0,\\ \sigma_\theta^e=\dfrac{u_{r_1}Er_1}{(1+\mu)r^2}+p_0.\end{cases} \tag{12}$$

Substituting $r=r_1$ into eq. (12) and combining eq. (5), the displacement at the elastoplastic interface can be obtained by

$$u_{r_1}=\frac{r_1(1+\mu)[p_0(\xi_0-1)+\sigma_q]}{E(1+\xi_0)}=D_0r_1. \tag{13}$$

Considering the geometric equations

$$\varepsilon_r=\frac{\mathrm{d}u_r}{\mathrm{d}r},\quad \varepsilon_\theta=\frac{u_r}{r}. \tag{14}$$

The strain solutions in the elastic region can be obtained by

$$\varepsilon_r^e=-\frac{D_0r_1^2}{r^2},\quad \varepsilon_\theta^e=\frac{D_0r_1^2}{r^2}. \tag{15}$$

3.2 Analytical solutions for the softening zone

In the softening zone, the total strain is the sum of the corresponding elastic and plastic strain components as

$$\begin{cases}\varepsilon_r=\varepsilon_r^e+\varepsilon_r^p,\\ \varepsilon_\theta=\varepsilon_\theta^e+\varepsilon_\theta^p,\end{cases} \tag{16}$$

where ε_r^p and ε_θ^p are the plastic components of the radial and circumferential strains in the softening zone, respectively.

The nonassociated flow rule in softening zone can be written as [5]

$$\varepsilon_r^p+h\varepsilon_\theta^p=0, \tag{17}$$

where h is the dilatancy coefficient of the softening zone and $h=(1+\sin\psi_0)/(1-\sin\psi_0)$ which is greater than 1 when considering the dilatancy effect of the rock mass and is equal to 1 without dilatancy. ψ_0 is the unified dilation angle in the softening zone.

By substituting eq. (16) to eq. (17) and using the displacement at the elastoplastic interface eq. (13), the general solution to the displacement in the softening zone can be obtained by

$$u=\frac{1}{r^h}\int_{r_1}^{r}r^h(\varepsilon_r^e+h\varepsilon_\theta^e)\mathrm{d}r+D_0r_1\left(\frac{r_1}{r}\right)^h. \tag{18}$$

Substituting $r=r_1$ into eq. (12), the radial stress at the elastoplastic interface can be obtained by

$$\sigma_r^p\Big|_{r=r_1}=\sigma_r^e\Big|_{r=r_1}=\frac{2p_0-\sigma_q}{\xi_0+1}. \tag{19}$$

By combining eqs. (5) and (8), the differential equation for the radial stress can be expressed as

$$\frac{\mathrm{d}\sigma_r}{\mathrm{d}r}+\frac{(1-\xi_0)\sigma_r}{r}=\frac{\sigma_q-E'\varepsilon_\theta^p}{r}. \tag{20}$$

To obtain the tunnel displacement and stresses in the softening zone, the elastic strains in the plastic zone should be determined first. For the simplicity of the solutions, there are mainly four different definitions of elastic strain used in theoretical analyses.

Case a: With ignoring the elastic strain in the softening zone [42–44], the radial displacement in the softening zone can be obtained by substituting $\varepsilon_r^e=\varepsilon_\theta^e=0$ into eq. (18) as

$$u=D_0r_1\left(\frac{r_1}{r}\right)^h. \tag{21}$$

By substituting eq. (21) into eq. (14) and considering eq. (16), the plastic strain components in softening zone can be written as

$$\varepsilon_r^p=-hD_0\left(\frac{r_1}{r}\right)^{h+1},\quad \varepsilon_\theta^p=D_0\left(\frac{r_1}{r}\right)^{h+1}. \tag{22}$$

Substituting eq. (22) into eq. (20) yields

$$r\frac{\mathrm{d}\sigma_r}{\mathrm{d}r}+(1-\xi_0)\sigma_r=\sigma_q-E'D_0\left(\frac{r_1}{r}\right)^{h+1}. \tag{23}$$

Integrating eq. (23) and considering the stress continuity condition at the elastoplastic interface eq. (18), the stresses in the softening zone can be expressed as

$$\begin{cases}\sigma_r=\left(\dfrac{r_1}{r}\right)^{1-\xi_0}\left[\dfrac{2p_0-\sigma_q}{\xi_0+1}-(\alpha_1+\beta_1)\right]+\alpha_1+\beta_1\left(\dfrac{r_1}{r}\right)^{h+1},\\ \sigma_\theta=\xi_0\left(\dfrac{r_1}{r}\right)^{1-\xi_0}\left[\dfrac{2p_0-\sigma_q}{\xi_0+1}-(\alpha_1+\beta_1)\right]+\alpha_1-\beta_1 h\left(\dfrac{r_1}{r}\right)^{h+1},\end{cases} \tag{24}$$

where $\alpha_1=\sigma_q/(1-\xi_0)$, and $\beta_1=E'D_0/(h+\xi_0)$.

Case b: With the assumption that the elastic strains are constant and equal to that of the elastoplastic interface [45,46], the elastic strain components can be written as

$$\varepsilon_r^e\big|_{r=r_1}=-D_0,\quad \varepsilon_\theta^e\big|_{r=r_1}=D_0. \tag{25}$$

By substituting eq. (25) into eq. (18), the displacement in the softening zone can be obtained by

$$u=\frac{D_0 r}{h+1}\left[2\left(\frac{r_1}{r}\right)^{h+1}+h-1\right]. \tag{26}$$

By substituting eq. (26) into eq. (14) and considering eq. (25), the circumferential plastic strain in softening zone can be written as

$$\varepsilon_\theta^p=\frac{2D_0}{h+1}\left[\left(\frac{r_1}{r}\right)^{h+1}-1\right]. \tag{27}$$

Substituting eq. (27) into eq. (20) yields

$$\frac{r\mathrm{d}\sigma_r}{\mathrm{d}r}+(1-\xi_0)\sigma_r=\sigma_q-\frac{2D_0E'}{h+1}\left[\left(\frac{r_1}{r}\right)^{h+1}-1\right]. \tag{28}$$

Integrating eq. (28) and considering eq. (19), the stresses in the softening zone can be expressed as

$$\begin{cases}\sigma_r=\left(\dfrac{r_1}{r}\right)^{1-\xi_0}\left[\dfrac{2p_0-\sigma_q}{\xi_0+1}-(\alpha_2+\beta_2)\right]+\alpha_2+\beta_2\left(\dfrac{r_1}{r}\right)^{h+1},\\ \sigma_\theta=\xi_0\left(\dfrac{r_1}{r}\right)^{1-\xi_0}\left[\dfrac{2p_0-\sigma_q}{\xi_0+1}-(\alpha_2+\beta_2)\right]+\alpha_2-\beta_2 h\left(\dfrac{r_1}{r}\right)^{h+1},\end{cases} \tag{29}$$

where $\alpha_2=\dfrac{(1+h)\sigma_q+2D_0E'}{(1-\xi_0)(1+h)}$, and $\beta_2=\dfrac{2D_0E'}{(h+\xi_0)(h+1)}$.

Case c: By considering the softening zone as a thick-walled cylinder subjected to (p_r-p_0) at the internal surface $r=r_2$ and (p_s-p_0) at the outer surface $r=r_1$ [47,48], the elastic strains in the softening zone can be written as

$$\begin{cases}\varepsilon_r^e=\dfrac{1+\mu}{E}\left[(1-2\mu)C_1+\dfrac{C_2r_1^2}{r^2}\right],\\ \varepsilon_\theta^e=\dfrac{1+\mu}{E}\left[(1-2\mu)C_1-\dfrac{C_2r_1^2}{r^2}\right],\end{cases} \tag{30}$$

where

$$\begin{cases}C_1=\dfrac{(p_s-p_0)r_1^2-(p_r-p_0)r_2^2}{r_1^2-r_2^2},\\ C_2=\dfrac{(p_r-p_s)r_2^2}{r_1^2-r_2^2},\end{cases} \tag{31}$$

where r_2 is the radius of the residual zone. p_r and p_s are the unified critical stresses referring to the initiation of the softening and residual zones respectively. The calculation method of p_r and p_s will be introduced later.

By substituting eq. (30) into eq. (18), the radial displacement in the softening zone can be obtained by

$$u=M_1\frac{r_1^{h+1}}{r^h}+\frac{M_2r^2-M_3r_2^2}{r}, \tag{32}$$

where $M_1=\dfrac{1+\mu}{E}[C_2-(1-2\mu)C_1]+D_0$, and $M_2=\dfrac{1+\mu}{E}(1-2\mu)C_1$, $M_3=\dfrac{1+\mu}{E}C_2\left(\dfrac{r_1}{r_2}\right)^2$.

By substituting eq. (32) into eq. (14) and considering eqs. (16) and (30), the circumferential plastic strain in the softening zone can be written as

$$\varepsilon_\theta^p=M_1\left(\frac{r_1}{r}\right)^{h+1}. \tag{33}$$

Similar to eq. (24), the stresses in the softening zone can be expressed as

$$\begin{cases}\sigma_r=\left(\dfrac{r_1}{r}\right)^{1-\xi_0}\left[\dfrac{2p_0-\sigma_q}{\xi_0+1}-(\alpha_3+\beta_3)\right]+\alpha_3+\beta_3\left(\dfrac{r_1}{r}\right)^{h+1},\\ \sigma_\theta=\xi_0\left(\dfrac{r_1}{r}\right)^{1-\xi_0}\left[\dfrac{2p_0-\sigma_q}{\xi_0+1}-(\alpha_3+\beta_3)\right]+\alpha_3-\beta_3 h\left(\dfrac{r_1}{r}\right)^{h+1},\end{cases} \tag{34}$$

where $\alpha_3=\sigma_q/(1-\xi_0)$, and $\beta_3=(E'M_1+D_0)/(h+\xi_0)$.

Case d: By using Hooke's law with considering the initial hydrostatic stress [49,50], the elastic strains can be expressed as

$$\begin{cases}\varepsilon_r^e=\dfrac{1-\mu^2}{E}\left[(\sigma_r-p_0)-\dfrac{\mu}{1-\mu}(\sigma_\theta-p_0)\right],\\ \varepsilon_\theta^e=\dfrac{1-\mu^2}{E}\left[(\sigma_\theta-p_0)-\dfrac{\mu}{1-\mu}(\sigma_r-p_0)\right].\end{cases} \tag{35}$$

By substituting eq. (35) into eq. (18) and then integrating, the radial displacement in the softening zone can be obtained by

$$u=\frac{1+\mu}{Er^h}\int_r^r r^h[(1-\mu-h\mu)\sigma_r+(h-h\mu-\mu)\sigma_\theta -(1-2\mu)(1+h)p_0]\mathrm{d}r+D_0r_1\left(\frac{r_1}{r}\right)^h. \tag{36}$$

Note that the derivation to eq. (36) requires stresses in the softening zone. Subsequently, by substituting eqs. (35) and (36) into eqs. (14) and (16) yields

$$\varepsilon_\theta^p=\frac{u}{r}-\frac{1-\mu^2}{E}\left[(\sigma_\theta-p_0)-\frac{\mu}{1-\mu}(\sigma_r-p_0)\right]. \tag{37}$$

Combining eq. (37) and eq. (5) yields

$$\varepsilon_\theta^p=\frac{Eu-(1+\mu)r[(\xi_0-\mu\xi_0-\mu)\sigma_r+\eta]}{\left[E'(1-\mu^2)+E\right]r}, \tag{38}$$

where $\eta=(1-\mu)\sigma_q+(2\mu-1)p_0$.

Substituting eq. (38) into eq. (20) yields

$$\frac{r\mathrm{d}\sigma_r}{\mathrm{d}r}+f(\sigma_r)=\sigma_q-\frac{E'(1+\mu)\eta}{E'\left(1-\mu^2\right)+E}, \tag{39}$$

where

$$f(\sigma_r)=\left(1-\xi_0\right)\sigma_r+\frac{E'Eu-E'(1+\mu)(\xi_0-\mu\xi_0-\mu)\sigma_r r}{\left[E'\left(1-\mu^2\right)+E\right]r}. \tag{40}$$

Integrating eq. (39) yields

$$\sigma_r=C\mathrm{e}^{-\int\frac{f(\sigma_r)}{r}\mathrm{d}r}+\mathrm{e}^{-\int\frac{f(\sigma_r)}{r}\mathrm{d}r}\int\frac{E'(1+\mu)\eta}{r[E'(1-\mu^2)+E]}\mathrm{e}^{\int\frac{f(\sigma_r)}{r}\mathrm{d}r}\mathrm{d}r, \tag{41}$$

where C is the constant which can be determined by using the boundary condition of eq. (19).

Subsequently, the radial displacement and stresses of the softening zone can be obtained by integrating eq. (41) in combination with eq. (36).

3.3 Analytical solutions for the residual zone

In the residual zone, the total strains can be written as

$$\begin{cases}\varepsilon_r=\varepsilon_r^s+\varepsilon_r^r,\\ \varepsilon_\theta=\varepsilon_\theta^s+\varepsilon_\theta^r,\end{cases} \tag{42}$$

where ε_r^s, ε_r^r and ε_θ^s, ε_θ^r are the softening and residual components of radial and circumferential strains in the residual zone, respectively.

The nonassociated flow rule in the residual zone can be written as [5]

$$\varepsilon_r^r+f\varepsilon_\theta^r=0, \tag{43}$$

where f is the dilatancy coefficient of the residual zone and $f=\left(1+\sin\psi_r\right)/\left(1-\sin\psi_r\right)$. ψ_r is the unified dilation angle in the residual zone. Based on the testing results obtained by Farmer [60], a range of $f=1.3-1.5$ is appropriate for soft rocks.

By substituting the displacement at the softening-residual interface into eqs. (42) and (43) and then integrating, the general solution to the displacement in the residual zone can be obtained by

$$u=\frac{1}{r^f}\int_{r_2}^{r}r^f\left(\varepsilon_r^s+f\varepsilon_\theta^s\right)\mathrm{d}r+u_{r_2}\left(\frac{r_2}{r}\right)^f, \tag{44}$$

where u_{r_2} is the radial displacement at the softening-residual interface.

By combining eqs. (6) and (8), the differential equation for the radial stress can be expressed as

$$\frac{r\mathrm{d}\sigma_r}{\mathrm{d}r}+\left(1-\xi_r\right)\sigma_r=\sigma_{qr}. \tag{45}$$

Integrating eq. (45) and considering the stress continuity condition at the softening-residual interface, the general solution to the stresses in the residual zone can be expressed as

$$\begin{cases}\sigma_r=\left(\sigma_{r_2}-\dfrac{\sigma_{qr}}{1-\xi_r}\right)\left(\dfrac{r}{r_2}\right)^{\xi_r-1}+\dfrac{\sigma_{qr}}{1-\xi_r},\\ \sigma_\theta=\xi_r\left(\sigma_{r_2}-\dfrac{\sigma_{qr}}{1-\xi_r}\right)\left(\dfrac{r}{r_2}\right)^{\xi_r-1}+\dfrac{\sigma_{qr}}{1-\xi_r}.\end{cases} \tag{46}$$

For Cases a, b and c, by substituting $r=r_2$ into eqs. (24), (29) and (34) and combining eq. (46), the stresses in the residual zone can be obtained by

$$\begin{cases}\sigma_r=\left\{\left(\dfrac{r_1}{r_2}\right)^{1-\xi_0}\left[\dfrac{2p_0-\sigma_q}{\xi_0+1}-\left(\alpha_i+\beta_i\right)\right]+\alpha_i+\beta_i\left(\dfrac{r_1}{r_2}\right)^{h+1}-\dfrac{\sigma_{qr}}{1-\xi_r}\right\}\left(\dfrac{r}{r_2}\right)^{\xi_r-1}+\dfrac{\sigma_{qr}}{1-\xi_r},\\ \sigma_\theta=\xi_r\left\{\left(\dfrac{r_1}{r_2}\right)^{1-\xi_0}\left[\dfrac{2p_0-\sigma_q}{\xi_0+1}-\left(\alpha_i+\beta_i\right)\right]+\alpha_i+\beta_i\left(\dfrac{r_1}{r_2}\right)^{h+1}-\dfrac{\sigma_{qr}}{1-\xi_r}\right\}\left(\dfrac{r}{r_2}\right)^{\xi_r-1}+\dfrac{\sigma_{qr}}{1-\xi_r},\end{cases} \tag{47}$$

where the subscript i ($i=1,\ 2,\ 3$) refers to the above-mentioned three cases respectively.

While for Case d, the stresses in the residual zone can be obtained by substituting $r=r_2$ into eq. (42) combining with eq. (46).

To obtain the displacement solution in the residual zone, four cases corresponding to the above derivation will be distinguished as well.

Case a: Ignoring the elastic strain in the residual zone, u_{r_2} can be given by substituting $r=r_2$ into eq. (20) as

$$u_{r_2}=D_0r_1\left(\frac{r_1}{r_2}\right)^h. \tag{48}$$

Substituting eq. (48) into eq. (44) and considering eqs. (13) and (20) yields

$$u=\frac{D_0r}{f+1}\left(\frac{r_1}{r_2}\right)^{h+1}\left[f-h+(h+1)\left(\frac{r_2}{r}\right)^{f+1}\right]. \tag{49}$$

Case b: By assuming that the elastic strains are equal to that of the softening-residual interface, the softening strain components can be obtained by combining eqs. (13) and (25) as

$$\begin{cases}\varepsilon_r^s\big|_{r=r_2}=\dfrac{D_0}{h+1}\left[h-1-2h\left(\dfrac{r_1}{r_2}\right)^{h+1}\right],\\ \varepsilon_\theta^s\big|_{r=r_2}=\dfrac{D_0}{h+1}\left[2\left(\dfrac{r_1}{r_2}\right)^{h+1}+h-1\right].\end{cases} \tag{50}$$

By substituting $r=r_2$ into eq. (25), u_{r_2} can be given as

$$u_{r_2}=\frac{D_0r_2}{h+1}\left[2\left(\frac{r_1}{r_2}\right)^{h+1}+h-1\right]. \tag{51}$$

Substituting eqs. (50) and (51) into eq. (44) yields

$$u=\frac{D_0 r}{(h+1)}\left[\frac{2f-2h}{f+1}\left(\frac{r_1}{r_2}\right)^{h+1}+h-1\right]+\frac{2D_0 r_2}{f+1}\left(\frac{r_1}{r_2}\right)^{h+1}\left(\frac{r_2}{r}\right)^{f}. \quad (52)$$

Case c: By using the thick-walled cylinder theory, the elastic strains in the residual zone can be written as

$$\begin{cases}\varepsilon_r^{\,e}=\dfrac{1+\mu}{E}\left[(1-2\mu)C_{1r}+\dfrac{C_{2r}r_2^2}{r^2}\right],\\ \varepsilon_\theta^{\,e}=\dfrac{1+\mu}{E}\left[(1-2\mu)C_{1r}-\dfrac{C_{2r}r_2^2}{r^2}\right],\end{cases} \quad (53)$$

where

$$\begin{cases}C_{1r}=\dfrac{(p_r-p_0)r_2^2-(p_i-p_0)r_0^2}{r_2^2-r_0^2},\\ C_{2r}=\dfrac{(p_i-p_r)r_0^2}{r_2^2-r_0^2}.\end{cases} \quad (54)$$

Substituting eq. (32) into eq. (14), then combining with eqs. (53) and (42) considering eq. (16), the softening components of the strains in the residual zone can be obtained as

$$\begin{cases}\varepsilon_r^{\,s}=M_{2r}+M_{3r}\dfrac{r_0^2}{r^2}-M_1 h\left(\dfrac{r_1}{r_2}\right)^{h+1}-M_2,\\ \varepsilon_\theta^{\,s}=M_{2r}+M_{3r}\dfrac{r_0^2}{r^2}+M_1\left(\dfrac{r_1}{r_2}\right)^{h+1},\end{cases} \quad (55)$$

where $M_{2r}=\dfrac{1+\mu}{E}(1-2\mu)C_{1r}$, and $M_{3r}=\dfrac{1+\mu}{E}C_{2r}\left(\dfrac{r_2}{r_0}\right)^2$.

The displacement on the softening-residual interface u_{r_2} can be given by substituting $r=r_2$ into eq. (31) as

$$u_{r_2}=M_1\frac{r_1^{h+1}}{r_2^{h}}+(M_2-M_3)r_2. \quad (56)$$

Substituting eqs. (53) and (54) into eq. (44) with integration, the radial displacement in the residual zone can be obtained by

$$\begin{aligned}u=&\frac{rN_r}{f+1}\left[1-\left(\frac{r_2}{r}\right)^{f+1}\right]+\frac{f+1}{f-1}M_{3r}\frac{r_0^2}{r}\left[1-\left(\frac{r_2}{r}\right)^{f-1}\right]\\&+\left[M_1\frac{r_1^{h+1}}{r_2^{h}}+(M_2-M_3)r_2\right]\left(\frac{r_2}{r}\right)^{f},\end{aligned} \quad (57)$$

where $N_r=(f+1)M_{2r}+(f-h)M_1\left(\dfrac{r_1}{r_2}\right)^{h+1}-M_2$.

Case d: By using the Hooke's law, the elastic strains can be obtained by eq. (35). Substituting eq. (32) into eq. (14), then combining with eqs. (35) and (42) considering eq. (16), the softening components of the strains in the residual zone can be obtained. Thereafter, the radial displacement in the residual zone can be obtained by substituting the softening components of the strains ($\varepsilon_r^{\,s}$ and $\varepsilon_\theta^{\,s}$) and the displacement at the softening-residual interface u_{r_2} into eq. (44). Notably, the softening components of the stresses require solving simultaneous equations, and the closed-form solution to the radial displacement in the residual zone cannot be obtained.

4 Analysis of the plastic radii and critical stresses

4.1 Analysis of the softening state

The radii of the softening and residual zones with the critical stresses p_s and p_r are derived in this section. Notably, the stresses of Cases a, b and c are in similar forms, their softening radii will be solved in a uniform manner, whereas Case d will be solved separately. Since the initial yielding of rock mass is defined by the yield criterion, it does not influence the definition of the elastic strains of the softening zone. By substituting eq. (5) to eq. (12) considering eq. (11), the unified initial yielding stress p_s can be obtained by

$$p_s=\frac{2p_0-\sigma_q}{1+\xi_0}. \quad (58)$$

Without the residual zone, the tunnel wall is in the softening state. For Cases a, b and c, by substituting $r=r_0$, $\sigma_r=p_i$ into eqs. (24), (29) and (34), the transcendental equation form of the softening radius can be expressed as

$$r_1=r_0\left\{\frac{p_i-\alpha_i}{\beta_i}-\left(\frac{r_1}{r_0}\right)^{1-\xi_0}\left[\frac{2p_0-\sigma_q}{(\xi_0+1)\beta_i}-\left(\frac{\alpha_i}{\beta_i}+1\right)\right]\right\}^{\frac{1}{h+1}}. \quad (59)$$

Based on eq. (59), the radii of the softening zone for all the cases can be obtained at given p_i. Notably, Case c, β_3 is a function of r_1 and the expressions of C_1 and C_2 should be rearranged as

$$\begin{cases}C'_1=\dfrac{(p_s-p_0)r_1^2-(p_i-p_0)r_0^2}{r_1^2-r_0^2},\\ C'_2=\dfrac{(p_i-p_s)r_0^2}{r_1^2-r_0^2}.\end{cases} \quad (60)$$

When the residual zone is about to appear ($p_i=p_r$), the tunnel wall $r=r_0$ is exactly at the softening-residual interface. Therefore, by substituting $r=r_0$ into eqs. (24), (29), and (34) and combining eq. (46) gives the transcendental equation form of the critical softening radii

$$\sigma_{qr}=\sigma_q-E'\varepsilon_\theta^{\,p}\big|_{r=r_0}+\sigma_{r_0}(\xi-\xi_r), \quad (61)$$

where σ_{r_0} can be given by substituting $r=r_0$ into eqs. (24), (29), and (34) as

$$\sigma_{r_0}=\left(\frac{r_1}{r_0}\right)^{1-\xi_0}\left[p_s-(\alpha_i+\beta_i)\right]+\alpha_i+\beta_i\left(\frac{r_1}{r_0}\right)^{h+1}. \quad (62)$$

Defining $n=r_1^*/r_0$ and then combining eqs. (61) and (62) considering eqs. (22), (27), and (33), the general transcendental equation form of n can be written as

$$N_1^* n^{h+1}+N_2^* n^{1-\xi_0}+N_3^*+\sigma_q-\sigma_{qr}=0, \quad (63)$$

where N_1^*, N_2^* and N_3^* are the undetermined coefficients related to the different cases as follows:

Case a:

$$N_1^* = \beta_1(\xi_0-\xi_r)-E'D_0,$$
$$N_2^* = \left[p_s-(\alpha_1+\beta_1)\right](\xi_0-\xi_r),$$
$$N_3^* = \alpha_1(\xi_0-\xi_r).$$

Case b:

$$N_1^* = \beta_2(\xi_0-\xi_r)-\frac{2D_0E'}{h+1},$$
$$N_2^* = \left[p_s-(\alpha_2+\beta_2)\right](\xi_0-\xi_r),$$
$$N_3^* = \alpha_2(\xi_0-\xi_r)+\frac{2D_0E'}{h+1}.$$

Case c:

$$N_1^* = \beta_3(\xi_0-\xi_r)-E'M_1,$$
$$N_2^* = \left[p_s-(\alpha_3+\beta_3^*)\right](\xi_0-\xi_r),$$
$$N_3^* = \alpha_3(\xi_0-\xi_r).$$

By substituting $r=r_0$, $\sigma_r=p_r$ into eqs. (24), (29), and (34) considering eq. (6), the critical stress p_r can be obtained by

$$p_r = \frac{1}{\xi_r+1}\left\{(1+\xi_0)\left(\frac{r_1^*}{r_0}\right)^{1-\xi_0}\left[p_s-(\alpha_i+\beta_i)\right] +2\alpha_i+(1-h)\beta_i\left(\frac{r_1^*}{r_0}\right)^{h+1}-\sigma_{qr}\right\}. \tag{64}$$

Evidently, the residual zone will exist only if the internal support pressure p_i is less than p_r.

While for Case c, using the boundary condition $p_i=p_r$ at $r_2=r_0$, the critical values of C_1 and C_2 in eq. (30) can be expressed as

$$\begin{cases} C_1^* = \dfrac{(p_s-p_0)\left(r_1^*\right)^2-(p_r-p_0)r_0^2}{\left(r_1^*\right)^2-r_0^2}, \\ C_2^* = \dfrac{(p_r-p_s)r_0^2}{\left(r_1^*\right)^2-r_0^2}. \end{cases} \tag{65}$$

The critical values of β_3 and M_1 in eq. (34) can be expressed as

$$\begin{cases} \beta_3^* = \dfrac{E'M_1^*+D_0}{h+\xi_0}, \\ M_1^* = \dfrac{1+\mu}{E}\left[C_2^*-(1-2\mu)C_1^*\right]+D_0. \end{cases} \tag{66}$$

For Case d, note that $f(\sigma_r)$ in eq. (41) is a function of r_1; thus, substituting $r=r_0$ and $\sigma_r=p_i$ into eq. (41), the softening radius r_1 can be obtained.

Considering that when the residual zone is about to appear, the boundary condition that $\sigma_{r_0}=p_r$ should be satisfied, substituting $\sigma_{r_0}=p_r$ into eq. (61) yields

$$p_r = \frac{\sigma_{qr}-\sigma_q+E'\varepsilon_\theta^p\big|_{r=r_0}}{(\xi-\xi_r)}. \tag{67}$$

By substituting $r=r_0$, $\sigma_r=p_r$ into eq. (41), the relationship between p_r and r_1^* can be given. Thereafter, in combination with eq. (67), the critical stress p_r and critical softening radius r_1^* which the residual zone is about to appear can be obtained.

4.2 Analysis of the residual state

In this section, the residual radii of Cases a, b and c will be solved in a uniform manner, whereas Case d will be solved separately.

When $p_i<p_r$, the radius of the residual zone will be greater than r_0. The boundary condition is $r=r_2$, $\sigma_r\big|_{r-dr}=\sigma_r\big|_{r+dr}$; substituting $r=r_2$ into eqs. (5) and (6) yields

$$\sigma_{qr} = \sigma_q-E'\varepsilon_\theta^p\big|_{r=r_2}+\sigma_{r_2}(\xi-\xi_r), \tag{68}$$

where σ_{r_2} of Cases a, b and c can be given by substituting $r=r_2$ into eq. (47) as

$$\sigma_{r_2} = \left(\frac{r_1}{r_2}\right)^{1-\xi_0}\left[p_s-(\alpha_i+\beta_i)\right]+\alpha_i+\beta_i\left(\frac{r_1}{r_2}\right)^{h+1}. \tag{69}$$

Defining $l=r_1/r_2$ and then combining eqs. (68) and (69) considering eqs. (22), (27), and (33), the general transcendental equation form of l can be written as

$$N_1l^{h+1}+N_2l^{1-\xi_0}+N_3+\sigma_q-\sigma_{qr}=0, \tag{70}$$

where the undetermined coefficients for the three cases are as follows:

Case a: $N_1=N_1^*$, $N_2=N_2^*$, $N_3=N_3^*$.

Case b: $N_1=N_1^*$, $N_2=N_2^*$, $N_3=N_3^*$.

Case c: $N_1=\beta_2(\xi-\xi_r)-E'M_1$,

$$N_2=\left[p_s-(\alpha_3+\beta_3)\right](\xi-\xi_r),\ N_3=\alpha_3(\xi-\xi_r).$$

By substituting the boundary condition $r=r_0$, $\sigma_r=p_i$ into eq. (47), the unified residual radii can be obtained as follows:

$$r_2 = r_0\left\{\frac{p_i-\dfrac{\sigma_{qr}}{1-\xi_r}}{l^{1-\xi_0}[p_s-(\alpha_i+\beta_i)]+\alpha_i+\beta_il^{h+1}-\dfrac{\sigma_{qr}}{1-\xi_r}}\right\}^{\frac{1}{1-\xi_r}}. \tag{71}$$

Notably, when the physical and mechanics parameters of the softening and residual zones are identical, eqs. (61) and (68) will be the same as those proposed by Fan et al. [61], and the solutions in Case b will degenerate to those of Fan's solutions. Moreover when $b=0$, the UST will degenerate to the M-C criterion; subsequently, the solutions to Case b can be transformed to those proposed by Yao et al. [53].

For Case d, eq. (68) can be transformed as

$$\sigma_{r_2}=\frac{\sigma_{qr}-\sigma_q+E'\varepsilon_\theta^p\big|_{r=r_2}}{\xi-\xi_r}. \tag{72}$$

Substituting $r=r_2$ into eq. (37) yields

$$\varepsilon_\theta^p\big|_{r=r_2}=\frac{u_{r_2}}{r_2}-\frac{1-\mu^2}{E}\left[(\sigma_\theta|_{r=r_2}-p_0)-\frac{\mu}{1-\mu}(\sigma_{r_2}-p_0)\right], \tag{73}$$

where u_{r_2} can be obtained by substituting $r=r_2$ into eq. (36).

Note that σ_{r_2} is the radial stress at the softening-residual interface, it can be obtained by substituting $r=r_2$ into eq. (41). Subsequently, in combination with eq. (72), the ratio of the softening and residual radii l can be given. Moreover, by substituting $r=r_0$, $\sigma_r=p_i$ into eq. (41), the residual radius r_2 in terms of p_i can be obtained. Thereafter, the softening radius can be obtained at a given p_i.

5 Validation of the proposed method

5.1 Comparison to the numerical simulations

To validate the proposed model, the results of the proposed method are compared with numerical simulations using the secondary development program of FLAC3D. Due to the algebraic complexity, a MATLAB program is compiled to carry out the computations for the analytical model. A deep circular tunnel of radius $r_0=6$ m with the burial depth of 400 m is considered here. The physical and mechanical parameters of the surrounding rock of $E=1.3$ GPa, $\mu=0.3$, $c_0=1$ MPa, $\varphi_0=30^\circ$, $c_r=0.7$ MPa, $\varphi_r=20^\circ$, $h=2.5$, $f=1.5$, $E'=400$ MPa, $b=0.5$, and $m=1$ are adopted for the analysis. The tunnel is subjected to a hydrostatic stress of $p_0=10$ MPa. Due to the symmetry of the analyzed problem, only a quarter of the tunnel is considered, as shown in Figure 4. Based on the proposed solutions, the ground reaction curves are obtained by gradually reducing the internal pressure p_i from 10 MPa to zero. A stress release function is conducted in the numerical simulation to get the tunnel displacements with a given support pressure. A total of three stages are foreseen in the calculation corresponding to the stress states of the surrounding rock.

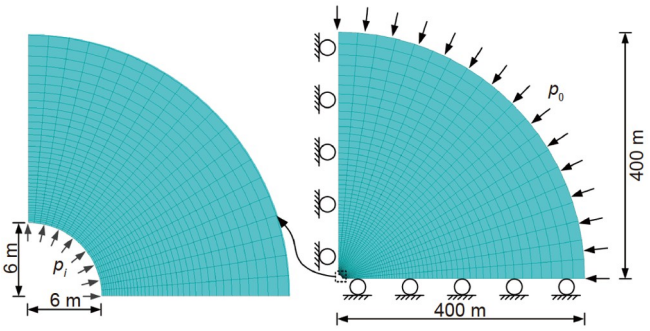

Figure 4 Numerical model used in the validation.

The results of the proposed method and the numerical simulations are shown in Figure 5. It is shown that the ground reaction curves from the proposed method of Case d match well with the numerical simulations, which means that the elastic strain definition in the numerical simulation is the Hooke's law. The plastic radii from the numerical simulations are slightly affected by the mesh division, which cannot be obtained accurately. While the critical support pressures regarding the elasto-plastic and softening-residual transition obtained by the proposed method is also in a good agreement with the results of the numerical simulations.

5.2 Comparison to the model test

5.2.1 *Model test layout*

As shown in Figure 6, the model test was conducted in a tank

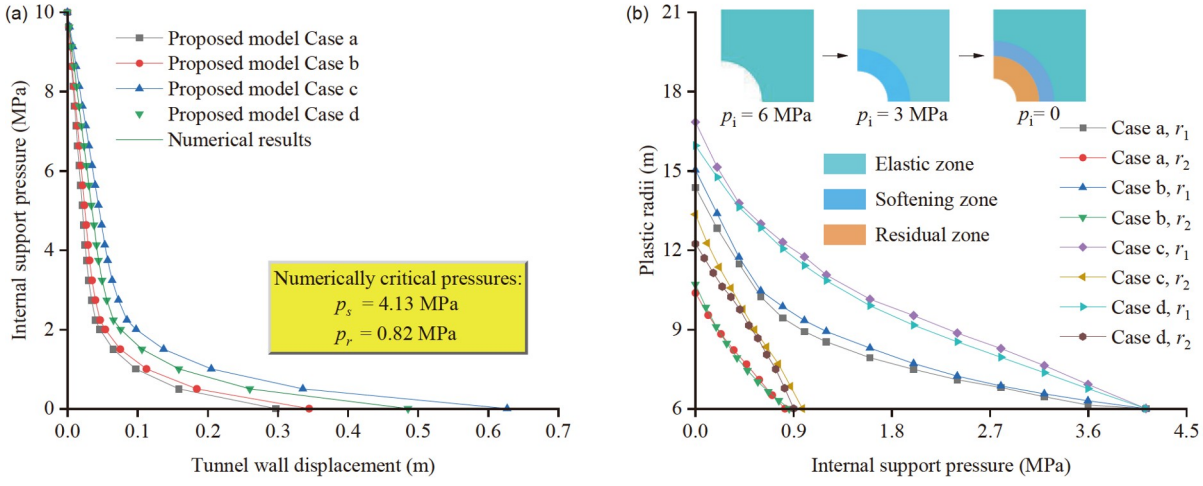

Figure 5 Validation of the proposed method by the numerical simulations. (a) Ground reaction curves; (b) analytically plastic radii and the numerical simulation results.

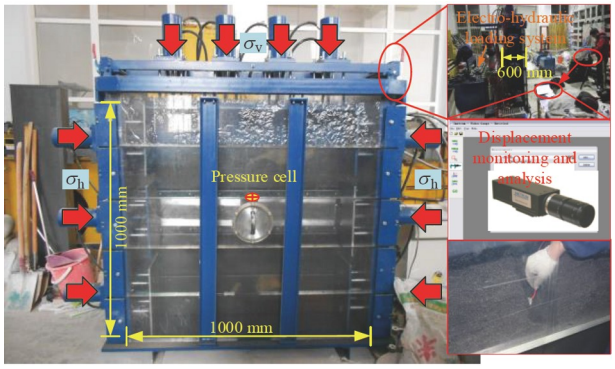

Figure 6 Overview of the model test.

with dimensions of 1000 mm × 1000 mm × 600 mm. The front wall was made by transparent organic glass, and the other sides were made by steel plate. A circular tunnel was installed in the middle of the tank with the diameter of 200 mm. According to the similarity principles, the similarity constant of the geometric dimension, stress, and elastic modulus are $C_l = C_\sigma = C_E = 70$, and the similarity constants for the unit weight, strain and Poisson's ratio are $C_\gamma = C_\varepsilon = C_\mu = 1$. This model test was aimed to illustrate the effect of the intermediate principal stress on the tunnel responses, the strain-softening behavior of the rock mass was not considered herein. Since the strain-softening model can degenerate to the elastic-perfectly plastic model, the model test can also be used to validate the proposed analytical solution. According to the refs. [62,63], we selected barite powders, quartz sand, vaseline and low-viscous lube to simulate the rock mass, of which the mixture ratio was 12:5:1.4:1. Through a set of compressive and shear tests, the physical and mechanical parameters of the model and prototype material are shown in Table 1.

The model test system is mainly composed of a loading system and data collection system. The vertical and horizontal pressures are applied by the top and the lateral loading systems respectively. To simulate the axisymmetric stress field, the vertical and horizontal pressures were set as $\sigma_v = \sigma_h = 80$ kPa, corresponding to the prototype *in-situ* stress of 5.6 MPa. The data collection system includes the stress measurement system and the displacement analysis system. The stress measurement was conducted by the earth pressure cells and the JC-4A static strain test system. In order to obtain the ground reaction curve, as well as explain the intermediate principal stress effect, the earth pressure cells were installed on the tunnel vault and both sides to monitor the radial, circumferential and the axial stresses. Since the pressure cells were installed closely with the small enough spacing, the stresses of different cells can be treated as the different stress components of a single point on the tunnel vault. The displacement measurement was carried out by a digital image correlation system, including a digital camera, a computer and the video gauge software (Figure 6).

The key processes of the model test are shown in Figure 7. The similar materials were mixed in a blender according to their weight ratios and then poured into the tank from the bottom to the top layer. After pouring a layer of materials, the corresponding glass plate was assembled and the ground was tamped by a rubber hammer. The earth pressure cells were

Table 1 The detailed parameters of the rock mass in the model test

Rock mass	Unit weight (kN/m^3)	Elastic modulus (MPa)	Poisson's ratio	Internal friction angle (°)	Cohesion (kPa)
Prototype	20.3	36.2	0.33	26.2	6.8
Similar material	20.3	2536.1	0.33	26.2	476.7

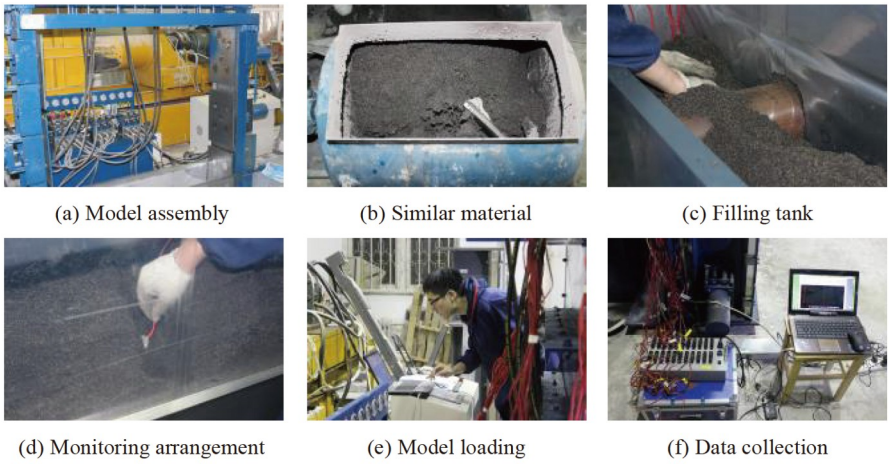

Figure 7 Key processes of the model tests.

buried at the designed locations. Then the horizontal and vertical pressures were applied at the same time, when they reached the designed values the pressures were kept constant. In model tests, the tunnel model was pulled out at a constant speed controlled by a hand instrument. The ground pressures and displacements are collected timely at the same time. To reduce the surface friction between the ground, the tunnel model was covered by a smooth reflective sheeting.

5.2.2 Comparison of the analytical solution and experimental results

Figure 8 shows the relationship between different directions of the surrounding rock pressures at the tunnel vault. Since the vertical and the horizontal pressure components are the minimum and maximum pressures σ_3 and σ_1 respectively at the tunnel vault, the relationship of the σ_1 and σ_3 are fitted herein. Moreover, the relationship of the sum of σ_3 and σ_1 with the intermediate principal stress σ_2 (axial stress) can be determined. Denoting the area that σ_1 increases with σ_3 as the plastic zone, then by substituting the coefficients of the fitted curves into eqs. (5) and (58), the intermediate principal stress coefficient b and the related parameter m can be determined as 0.49 and 0.98 of the prototype respectively. In this regard, the model test can be served as an alternative approach to determining the intermediate principal stress coefficient.

When the peak strength and the residual strength of the rock mass are identical, the proposed solutions will degenerate to the elastic-perfectly plastic solutions. Then by substituting the values of b and m into the proposed solutions, the ground reaction curves can be obtained. Figure 9 shows the results from the analytical model and the model test. It can be seen that the solution of Case d matches best with the model test, which is the exact one. The maximum tunnel displacement from Case c is a little greater than that from model test with the relative error of 5.7%, which can be used in the tunnel design from the safety viewpoint. The results from solutions of Cases a and b are much smaller than those from the model test, which should be carefully evaluated for solving a particular problem.

5.3 Comparison to the existing analytical models

To investigate the effect of different definitions of the elastic strains and highlight the advantages of the proposed method in engineering applications, the proposed analytical solutions are compared with the models proposed by Yao et al. [53] and Zhang et al. [54]. Since Zhang's solution is based on the UST elastic-brittle-plastic model with three definitions of the elastic strains, the results obtained by Zhang's model are based on the softening parameters. The physical and mechanical parameters of the rock mass are the same as Sect. 5.1. To better compare the proposed method and the existing models, the dimensionless values of the calculated results are

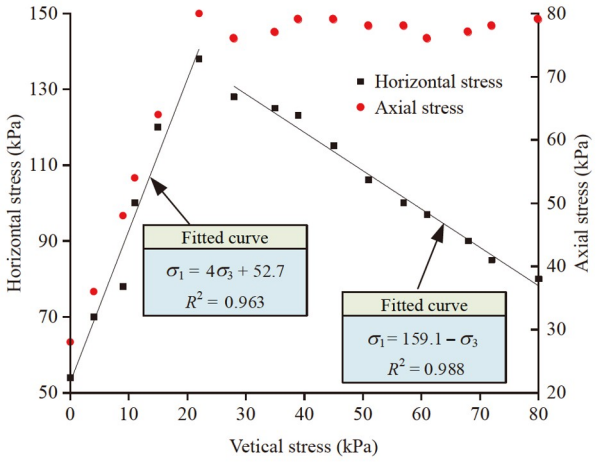

Figure 8 Surrounding rock pressure components at the tunnel vault from model test.

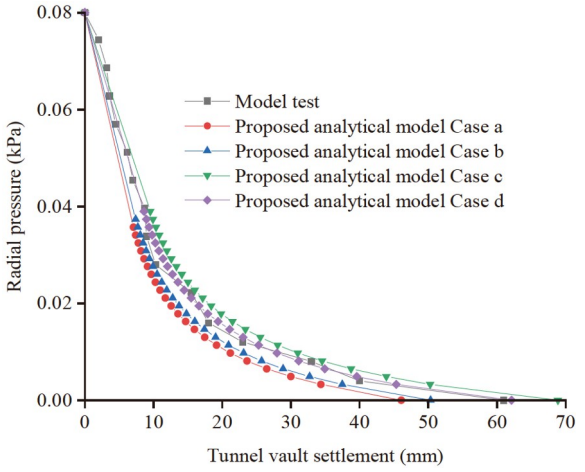

Figure 9 Comparison of the analytical solutions with the model test.

used here. The displacement and plastic radii are normalized by the tunnel radius, and the stress is normalized by the in-situ stress.

Figure 10 shows the dimensionless tunnel displacements of the above-mentioned four cases with the internal support pressure $p_i = 0$. The tunnel displacements of Case a are the lowest, while Case c gives the highest displacements. On the tunnel boundary, the displacement of Case c is more than twice that of Case a. The displacements given by Case b fall in between those given by Cases c and d, while they are closer to that given by Case a. Cases a and b may underestimate the tunnel displacement, particularly for tunnels excavated in soft rocks, which should be carefully evaluated in tunnel design. As the exact one, Case d is a little lower than Case c, which could not yield a specific solution for the tunnel displacement. In terms of tunnel safety and calculation simplicity, Case c is appropriate for solving a particular problem. Moreover, the comparison between the proposed method and Yao's solution shows that the M-C criterion

overestimates the tunnel displacement without considering the effect of the intermediate principal stress. This means that the M-C criterion may underestimate the rock mass strength, which unnecessarily increases the support cost. Moreover, it shows that the tunnel displacements from the proposed method are greater than those from the Zhang's solution in all the cases. Therefore, Zhang's model should be carefully evaluated for rock masses exhibiting strain-softening behavior, particularly for average-quality rocks. The proposed model thus excels in solving the mentioned problem over the classical models.

Figure 11 shows the dimensionless stresses with the internal support pressure $p_i = 0$. As shown, the radial stresses in the residual zone are the same in the four cases. The peak values of the circumferential stresses given by Cases b, c and d are nearly equal, which are greater that of Case a. In comparison, the positions where the peak values are located are quite different, which means that the radii of the softening and residual zones differ. The area where the circumferential stress increases in Case c is the largest and that in Case a is the smallest close to Case b. In comparison, the area obtained by the M-C criterion is much larger than that obtained by the proposed method. This once again proves the importance of considering the effect of the intermediate principal stress. A comparison shows that the peak values of σ_θ obtained from Zhang's model are slightly greater than those obtained from the proposed model. In addition, the radial stresses of all the cases are slightly different, and the definitions of the elastic strains have relatively less effect on the radial stresses.

The radii of the softening and residual zones can be obtained by gradually reducing the internal support pressure p_i, as shown in Figure 12. The initial yielding stresses p_s of the four cases are identical, while the softening-residual critical stress p_r of Case c is the highest, indicating that the residual zone appears earlier with the stress release. The radii of the softening and residual zones of Case c are also greater than those of the other three cases. A comparison of the proposed method and Yao's solution shows that the critical stresses, and the radii of the softening and residual zones obtained by the M-C criterion are greater than those obtained by the UST. Therefore, it can be concluded that the UST takes full advantages of the rock mass strength, which is beneficial to reduce the project cost. Zhang's model includes one single plastic zone, and the plastic radius r_p is free from the definition of elastic strain. r_p from Zhang's model is significantly greater than those from the proposed model in all the cases.

6 Parametric analysis

In this section, an extensive parametric analysis is conducted to investigate the effects of the intermediate principal stress,

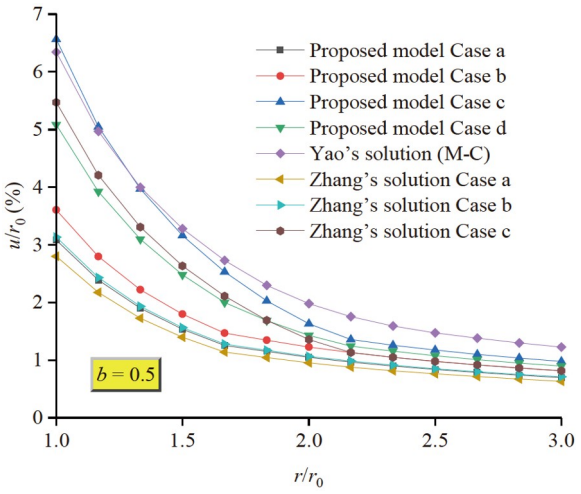

Figure 10 Dimensionless tunnel displacements with different definitions of the elastic strain.

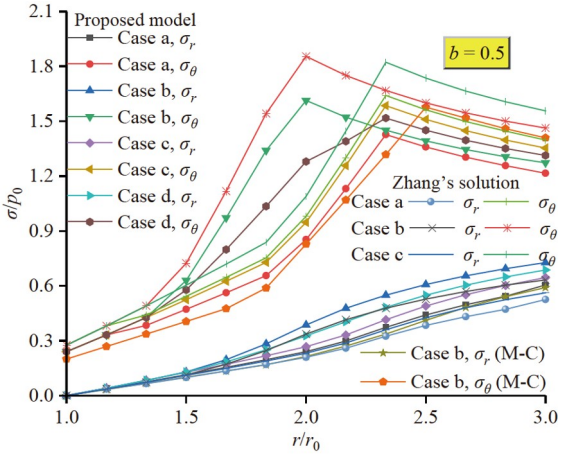

Figure 11 Dimensionless stresses with different definitions of the elastic strain.

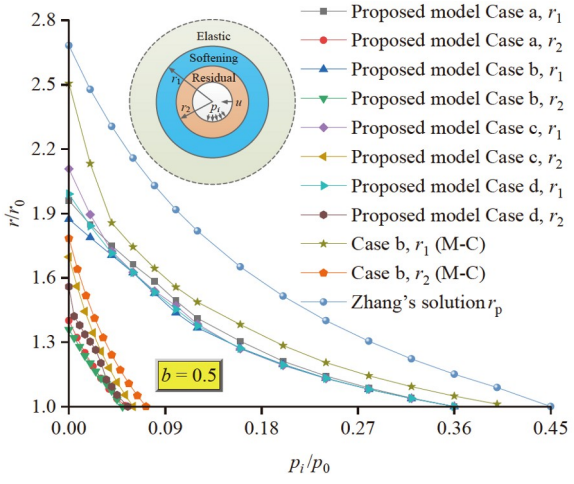

Figure 12 Dimensionless softening and residual radii with different definitions of the elastic strain.

the dilatancy property, and softening and residual degrees on the tunnel responses. The typical values of b, h, E', c_r and φ_r are adopted for the analysis, as listed in Table 2. When studying the influence of one single parameter, the other parameters take the fiducial values of Table 2. As mentioned above, Case c is the most appropriate assumption for soft rocks, it is chosen as the example herein. Notably, the intension here is not to study all the influential parameters, but to explore the different tunnel responses under the effect of the intermediate principal stress and to prove the necessity for considering the difference between the softening and residual zones, which was not included in the existing studies.

Figure 13 shows the effect of the intermediate principal stress with different softening dilatancy properties of the rock mass. With the increase in b, the tunnel displacement and the radii of the softening and residual zones decrease to different degrees. The greater the h value, the more significant the effect of the intermediate principal stress. Taking $h = 1$ and $h = 3$ as examples, the tunnel displacement and the radii of the softening and residual zones decrease by 50% and 57%, 26% and 32%, 31% and 31%, respectively, when $b = 0$ compared with those when $b = 1$. This indicates that the greater the dilatancy of the surrounding rock, the more important it is to consider the intermediate principal stress. Therefore, the effect of the intermediate principal stress should be considered reasonably in practical engineering applications. The value of b can be obtained by geological exploration combined with true triaxial test, laboratory model test and numerical simulation [58,64]. The analysis of Figure 13 also shows that the softening dilatancy has a certain influence on the tunnel responses. With the increase in h, the tunnel displacement and radius of the softening zone increase significantly, whereas the radius of the residual zone almost remains unchanged.

Table 2 Fiducial values and variation ranges of the parameters

Parameter	Fiducial value	Variation range
b	0.5	0, 0.25, 0.5, 0.75, 1
h	1.35	1.3, 1.35, 1.4, 1.45, 1.5
E' (MPa)	400	200, 400, 600, 800, 1000
c_r (MPa)	0.7	0.6, 0.7, 0.8, 0.9, 1.0
φ_r (°)	20	10, 15, 20, 25, 30

The dimensionless tunnel displacements, stresses, and radii of the softening and residual zones under different softening degrees represented here by the softening modulus E' are plotted in Figure 14. As shown in Figure 14, with the decrease in E', the tunnel displacement, maximum circumferential stress, and stress-increasing area increase significantly. Interestingly, E' does not influence the stresses in the residual zone, while it affects the residual radius. Owing to the increase in E', the radii of the softening and residual zones decrease, so does their ratio. According to Jiang et al. [56] and Zhang and Chen [65], the greater the residual radius, the lower the stability of the surrounding rock and the more difficult it is to control. Therefore, by controlling the softening degree of the surrounding rock, the radius of the residual zone can be reduced, which is beneficial to tunnel safety.

Figures 15 and 16 show the tunnel responses varying with the mechanical parameters in the residual zone c_r and φ_r with different residual dilatancy f. With the increase in c_r and φ_r, the tunnel displacements and radii of the softening and residual zones reduce dramatically. The values of c_r and φ_r not only affect the response of the residual zone, but also has a significant effect on the softening zone. The ratio of the softening and residual radii decreases with c_r and φ_r, which means that the elastoplastic and softening-residual interfaces get closer. When $\varphi_r = \varphi_0 = 30°$, the radii of the residual and

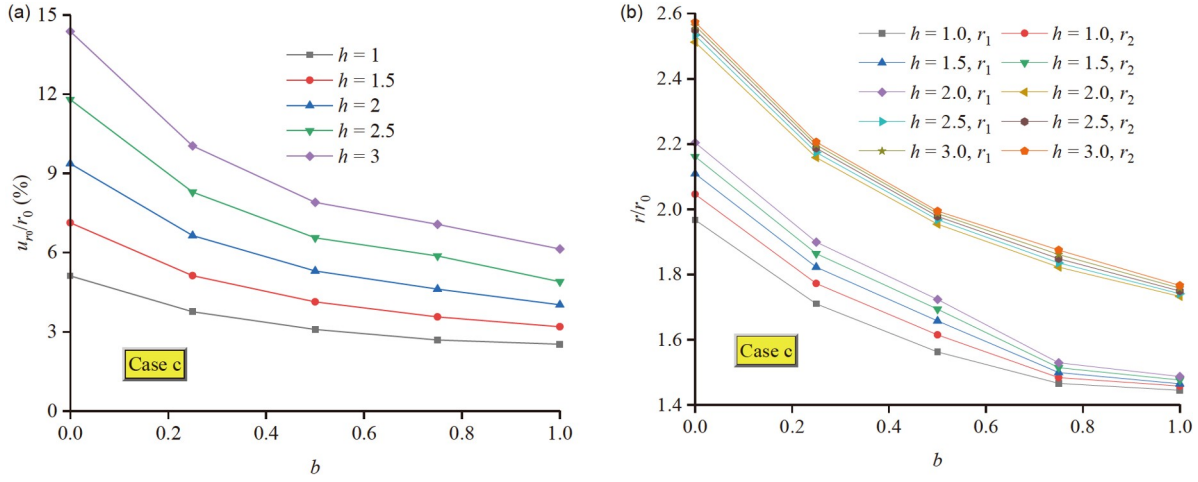

Figure 13 Effect of the intermediate principal stress under different softening dilatancy. (a) Dimensionless tunnel displacements; (b) dimensionless plastic radii.

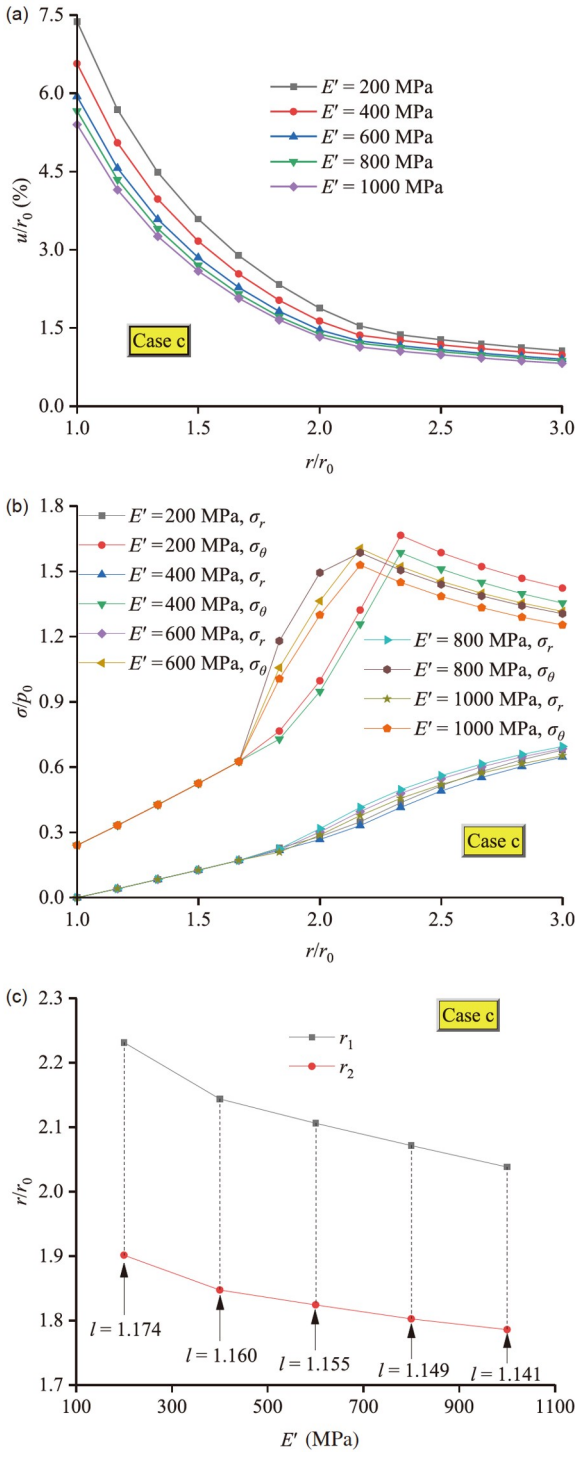

Figure 14 Effect of the softening modulus on tunnel responses. (a) Dimensionless tunnel displacements; (b) dimensionless stresses; (c) dimensionless plastic radii.

softening zones are almost equal. Figures 15 and 16 also show that with the increase in f from 1.35 to 1.5, the tunnel displacement increases slightly, while the radii of the softening and residual zones remain stable, showing no relationship with increasing f. Moreover, when c_r and φ_r increase, the influence of f on the tunnel displacement becomes more limited. This result indicates that, the greater the residual strength, the weaker the effect of the residual dilatancy. Therefore, the mechanical parameters in the residual zone should be identified carefully rather than considering them as those of the softening zone. According to the convergence-confinement method, the existing models would lead to unsafe tunnel design. The existing models should be used with caution in solving a particular problem. The proposed solutions thus excel in tunnel design over the existing models.

7 Conclusions

In this study, the analytical solutions for the responses of deep circular tunnels excavated in rock masses exhibiting strain-softening behavior were derived based on the unified strength theory. The difference in the definitions of the elastic strain was illustrated for strain-softening rock masses. A parametric study with the proposed solutions was performed to investigate the effects of the intermediate principal stress and mechanical parameters of the residual zone on tunnel responses. The main conclusions can be summarized as follows.

(1) Based on the UST and different definitions of the elastic strain, solutions to the tunnel displacements, stresses, plastic radii and critical stresses considering the effect of the intermediate principal stress were deduced. The proposed solutions were further used for obtaining the ground reaction curve, the results from the proposed model matched well with the model test and numerical simulations, thus permitting its application in the convergence-confinement method for tunnels excavated in strain-softening rock mass.

(2) Among the four definitions of the elastic strain, Case a yielded the lowest tunnel displacements and plastic radii. The calculated values of Case b were slightly greater and close to those of Case a, which also underestimated the tunnel responses. The results of Case d were found to match best with the model test, which can be treated as the exact solution. Case c yielded the highest tunnel displacements and plastic radii, slightly greater than the exact one (Case d) without explicit solution. In view of tunnel safety and computing simplicity, solutions based on Case c were found to be the most appropriate for practical applications in engineering design.

(3) The calculated values of the tunnel displacements and plastic radii by UST were lower than those obtained by the M-C criterion, indicating that the M-C criterion overestimated the tunnel responses. The effect of intermediate principal stress helps prevent the surrounding rock from yielding and resisting tunnel displacement. The greater the intermediate principal stress coefficient b, the lower the tunnel displacements and plastic radii. Therefore, the effect

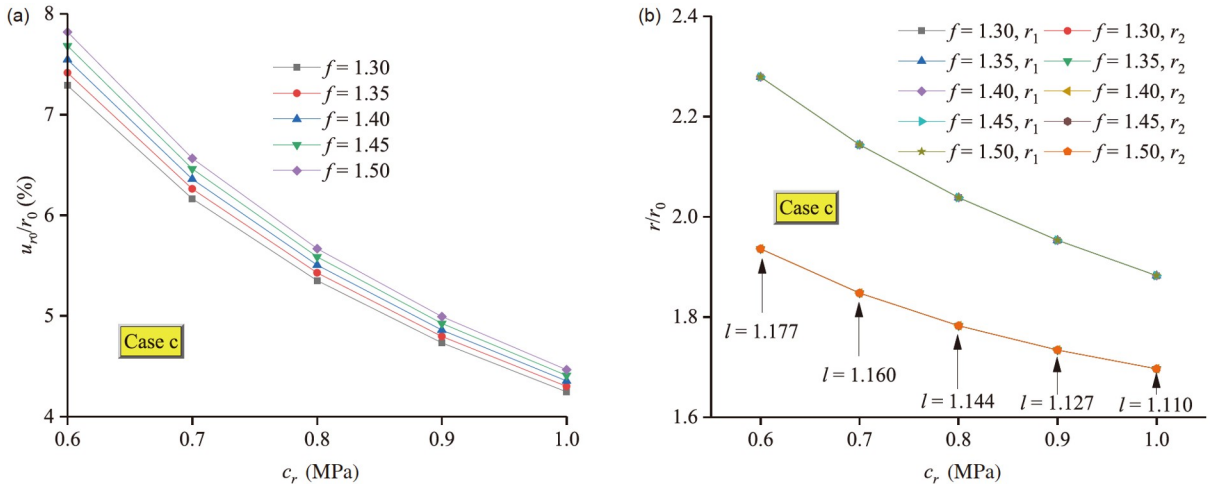

Figure 15 Effect of the residual cohesion under different residual dilatancy. (a) Dimensionless tunnel displacement; (b) dimensionless plastic radii.

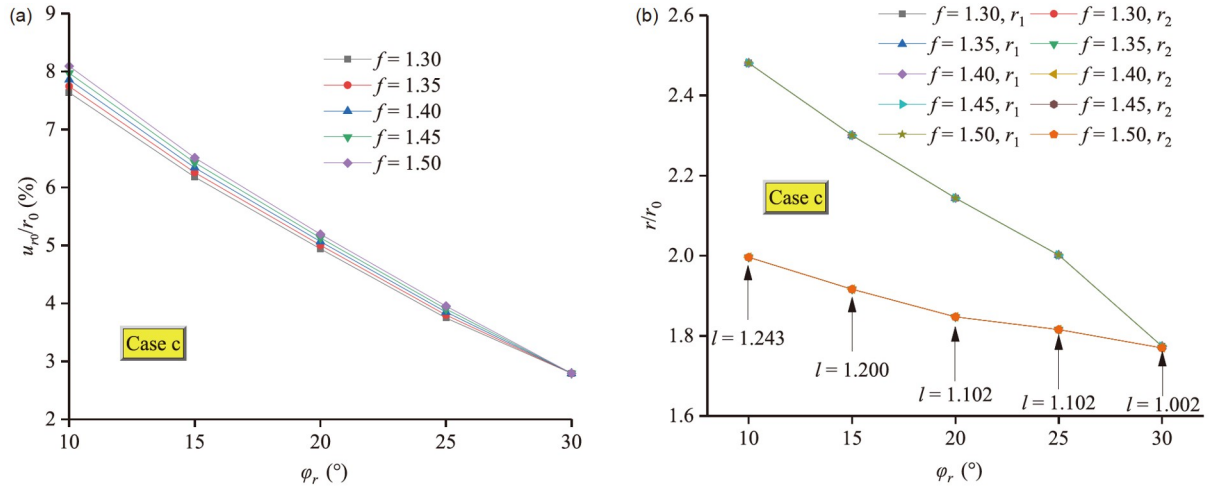

Figure 16 Effect of the residual friction angle under different residual dilatancy. (a) Dimensionless tunnel displacement; (b) dimensionless plastic radii.

of intermediate principal stress helps fully utilize the strength of rock masses, which is beneficial to reduce the support cost and cannot be neglected. Appropriate values of b should be determined for different materials in practical engineering, and the presented model test can be served as an alternative approach to determine the intermediate principal stress.

(4) To highlight the significance of different parameters, which most of the existing solutions neglected, a parametric study was performed. The softening modulus and softening dilatancy showed a significant effect on the tunnel responses, while the softening dilatancy had a negligible effect on the residual radius. The effects of the mechanical parameters in the residual zone on the tunnel responses were remarkable, while the influence of the residual dilatancy was quite limited under a high residual strength. Therefore, the proposed model outperformed the existing solutions using the UST elastic-brittle-plastic model in solving the mentioned problem for average-quality rocks.

This work was supported by the Fundamental Research Funds for the Central Universities (Grant No. 2021RC202), and the National Natural Science Foundation of China (Grant No. 51738002).

1 Oreste P P. The convergence-confinement method: Roles and limits in modern geomechanical tunnel design. Am J Appl Sci, 2009, 6: 757–771
2 Mahdevari S, Torabi S R. Prediction of tunnel convergence using artificial neural networks. Tunnelling Underground Space Tech, 2012, 28: 218–228
3 Fang Q, Zhang D, Zhou P, et al. Ground reaction curves for deep circular tunnels considering the effect of ground reinforcement. Int J Rock Mech Min Sci, 2013, 60: 401–412
4 Di Q, Li P, Zhang M, et al. Three-dimensional theoretical analysis of seepage field in front of shield tunnel face. Underground Space, 2022, 7: 528–542
5 Brown E T, Bray J W, Ladanyi B, et al. Ground response curves for rock tunnels. J Geotech Engrg, 1983, 109: 15–39
6 Carranza-Torres C, Fairhurst C. The elasto-plastic response of underground excavations in rock masses that satisfy the Hoek-Brown failure criterion. Int J Rock Mech Min Sci, 1999, 36: 777–809
7 Li P, Fang Q, Zhang D. Analytical solutions of stresses and dis-

placements for deep circular tunnels with liners in saturated ground. J Zheijang Univ-Sci, 2014, 15: 395–404
8 Guan Z, Jiang Y, Tanabasi Y. Ground reaction analyses in conventional tunnelling excavation. Tunnelling Underground Space Tech, 2007, 22: 230–237
9 Han J, Li S, Li S, et al. A procedure of strain-softening model for elasto-plastic analysis of a circular opening considering elasto-plastic coupling. Tunnelling Underground Space Tech, 2013, 37: 128–134
10 Cui L, Zheng J J, Dong Y K, et al. Prediction of critical strains and critical support pressures for circular tunnel excavated in strain-softening rock mass. Eng Geol, 2017, 224: 43–61
11 Luo J W, Zhang D L, Fang Q, et al. Analytical study on pretensioned bolt-cable combined support of large cross-section tunnel. Sci China Tech Sci, 2020, 63: 1808–1823
12 Papanastasiou P, Durban D. Elastoplastic analysis of cylindrical cavity problems in geomaterials. Int J Numer Anal Meth Geomech, 1997, 21: 133–149
13 Leu S Y. Analytical and numerical investigation of strain-hardening viscoplastic thick-walled cylinders under internal pressure by using sequential limit analysis. Comput Methods Appl Mech Eng, 2007, 196: 2713–2722
14 Zhang Q, He W, Wang H Y, et al. Elasto-plastic solutions for expanding cavities in strain-hardening and/or softening soils. Tunnelling Underground Space Tech, 2021, 107: 103660
15 Sharan S K. Exact and approximate solutions for displacements around circular openings in elastic-brittle-plastic Hoek-Brown rock. Int J Rock Mech Min Sci, 2005, 42: 542–549
16 Chen R, Tonon F. Closed-form solutions for a circular tunnel in elastic-brittle-plastic ground with the original and generalized Hoek-Brown failure criteria. Rock Mech Rock Eng, 2011, 44: 169–178
17 Wang S, Wu Z, Guo M, et al. Theoretical solutions of a circular tunnel with the influence of axial in situ stress in elastic-brittle-plastic rock. Tunnelling Underground Space Tech, 2012, 30: 155–168
18 Miao J B, Lu D C, Lin Q T, et al. Time-dependent surrounding soil pressure and mechanical response of tunnel lining induced by surrounding soil viscosity. Sci China Tech Sci, 2021, 64: 2453–2468
19 Lu D C, Miao J B, Du X L, et al. A new method of developing elastic-plastic-viscous constitutive model for clays. Sci China Tech Sci, 2020, 63: 303–318
20 Lu D C, Miao J B, Du X L, et al. A 3D elastic-plastic-viscous constitutive model for soils considering the stress path dependency. Sci China Technol Sci, 2020, 63: 791–808
21 Mogi K. Effect of the intermediate principal stress on rock failure. J Geophys Res, 1967, 72: 5117–5131
22 Singh B, Goel R K, Meharotra V K, et al. Effect of intermediate principal stress on strength of anisotropic rock mass. Tunn Undergr Space Technol, 1998, 13: 71–79
23 Xu S Q, Yu M H. The effect of the intermediate principal stress on the ground response of circular openings in rock mass. Rock Mech Rock Engng, 2006, 39: 169–181
24 Zhang C, Zhang Q, Zhao J, et al. Unified analytical solutions for a circular opening based on non-linear unified failure criterion. J Zhejiang Univ Sci A, 2010, 11: 71–79
25 Yao Y P, Cui W J, Wang N D. Three-dimensional dissipative stress space considering yield behavior in deviatoric plane. Sci China Tech Sci, 2013, 56: 1999–2009
26 Xiao Y, Liu H L, Liu H, et al. Unified plastic modulus in the bounding surface plasticity model. Sci China Tech Sci, 2016, 59: 932–940
27 Zhang D, Sun Z, Fang Q. Scientific problems and research proposals for Sichuan-Tibet railway tunnel construction. Underground Space, 2022, 7: 419–439
28 Yu M H, Li J C, Zhang Y Q. Unified characteristics line theory of spacial axisymmetric plastic problem. Sci China Ser E-Technol Sci, 2001, 44: 207–215
29 Yu M H, Zan Y W, Zhao J, et al. A unified strength criterion for rock material. Int J Rock Mech Min Sci, 2002, 39: 975–989
30 Mohammadi H, Farsangi M, Jalalifar H, et al. Influence of gravity loading on the ground reaction curve at tunnel crown based on the nonlinear unified strength criterion. Int Res J Appl Basic Sci, 2013, 6: 563–571
31 Ma Z Y, Liao H J, Dang F N. Effect of intermediate principal stress on flat-ended punch problems. Arch Appl Mech, 2014, 84: 277–289
32 Kang X, Liao H, Leng X. An enhanced bounding surface plasticity model for soft rock subjected to drained and undrained condition. Comput Geotechnics, 2020, 127: 103742
33 Ma G, Hao H, Iwasaki S. Unified plastic limit analyses of circular plates under arbitrary load. J Appl Mech, 1999, 66: 568–570
34 Yao Y, Lu D, Zhou A. Generalized non-linear strength theory and transformed stress space. Sci China Ser E, 2004, 47: 691–709
35 Liao H, Ma Z, Su L. Calculation of the ultimate bearing capacity of soil slope based on the unified strength theory. Int J Mod Phys B, 2008, 22: 5637–5642
36 Wang Y, Yu M, Xiao Y, et al. Dynamic plastic response of a circular plate based on unified strength theory. Int J Impact Eng, 2005, 31: 25–40
37 Zhang C, Zhao J, Zhang Q, et al. A new closed-form solution for circular openings modeled by the unified strength theory and radius-dependent Young's modulus. Comput Geotech, 2012, 42: 118–128
38 Fan W, Yu M, Deng L, et al. New strength formulae for rock surrounding a circular opening. Can Geotech J, 2013, 50: 735–743
39 Li N S, Tang B, Xie L H. Slope stability analysis of earth-rockfill dams using MGA and UST. J Comput Eng, 2015, 2015: 895142
40 Huang X, Zhang J, Yang L, et al. Elasto-plastic analysis of the surrounding rock mass in circular tunnel based on the generalized nonlinear unified strength theory. Int J Min Sci Tech, 2016, 26: 819–823
41 Ghorbani A, Hasanzadehshooiili H. A comprehensive solution for the calculation of ground reaction curve in the crown and sidewalls of circular tunnels in the elastic-plastic-EDZ rock mass considering strain softening. Tunnelling Underground Space Tech, 2019, 84: 413–431
42 Hughes J M O, Wroth C P, Windle D. Pressuremeter tests in sands. Géotechnique, 1977, 27: 455–477
43 Li P, Wang F, Fang Q. Undrained analysis of ground reaction curves for deep tunnels in saturated ground considering the effect of ground reinforcement. Tunnelling Underground Space Tech, 2018, 71: 579–590
44 Zhao C, Wang Y B, Zhao C, et al. Analysis of drained cavity unloading-contraction considering different degrees of intermediate principal stress with unified strength theory. Int J Geomech, 2020, 20
45 Wang Y. Ground response of circular tunnel in poorly consolidated rock. J Geotechn Eng, 1996, 122: 7032018708
46 Park K H, Kim Y J. Analytical solution for a circular opening in an elastic-brittle-plastic rock. Int J Rock Mech Min Sci, 2006, 43: 616–622
47 Reed M B. Stresses and displacements around a cylindrical cavity in soft rock. IMA J Appl Math, 1986, 36: 223–245
48 Sharan S K. Elastic-brittle-plastic analysis of circular openings in Hoek-Brown media. Int J Rock Mech Min Sci, 2003, 40: 817–824
49 Lv A, Masoumi H, Walsh S D C, et al. Elastic-softening-plasticity around a borehole: An analytical and experimental study. Rock Mech Rock Eng, 2019, 52: 1149–1164
50 Sun Z, Zhang D, Fang Q, et al. Analysis of the interaction between tunnel support and surrounding rock considering pre-reinforcement. Tunnelling Underground Space Tech, 2021, 115: 104074
51 Cai M, Kaiser P K, Tasaka Y, et al. Determination of residual strength parameters of jointed rock masses using the GSI system. Int J Rock Mech Min Sci, 2007, 44: 247–265
52 Alejano L R, Rodriguez-Dono A, Alonso E, et al. Ground reaction curves for tunnels excavated in different quality rock masses showing several types of post-failure behaviour. Tunnelling Underground Space Tech, 2009, 24: 689–705
53 Yao G S, Li J P, Gu S C. Analytic solution to deformation of soft rock tunnel considering dilatancy and plastic softening of rock mass (in Chinese). Rock Soil Mech, 2009, 30: 463–467

54 Zhang C G, Wang J F, Zhao J H. Unified solutions for stresses and displacements around circular tunnels using the Unified Strength Theory. Sci China Tech Sci, 2010, 53: 1694–1699
55 Alonso E, Alejano L R, Varas F, et al. Ground response curves for rock masses exhibiting strain-softening behaviour. Int J Numer Anal Meth Geomech, 2003, 27: 1153–1185
56 Jiang Y, Yoneda H, Tanabashi Y. Theoretical estimation of loosening pressure on tunnels in soft rocks. Tunnelling Underground Space Tech, 2001, 16: 99–105
57 Cai Y, Jiang Y, Djamaluddin I, et al. An analytical model considering interaction behavior of grouted rock bolts for convergence-confinement method in tunneling design. Int J Rock Mech Min Sci, 2015, 76: 112–126
58 Yu M H. Unified strength Theory and Its Applications. 2nd ed. Singapore: Springer, 2018
59 Sun Z Y, Zhang D L, Fang Q, et al. Spatial and temporal evolution characteristics of interaction between primary support and tunnel surrounding rock (in Chinese). Chin J Rock Mech Eng, 2017, 36: 3943–3956
60 Farmer I W. Engineering Properties of Rocks. London: Butler & Tanner, 1968
61 Fan W, Yu M H, Chen L, et al. Unified elastoplastic solution for surrounding rocks of openings with consideration of material dilatancy and softening (in Chinese). Chin J Rock Mech Eng, 2004, 23: 3213–3220
62 Zheng H, Li P, Ma G, et al. Experimental investigation of mechanical characteristics for linings of twins tunnels with asymmetric cross-section. Tunnelling Underground Space Tech, 2022, 119: 104209
63 Li L, Shang C, Chu K, et al. Large-scale geo-mechanical model tests for stability assessment of super-large cross-section tunnel. Tunnelling Underground Space Tech, 2021, 109: 103756
64 Deng L, Fan W, Yu M. Parametric study of a loess slope based on unified strength theory. Eng Geol, 2018, 233: 98–110
65 Zhang D L, Chen L P. Compound structural characteristics and load effect of tunnel surrounding rock (in Chinese). Chin J Rock Mech Eng, 2016, 35: 456–469